ACS APPLIED MATERIALS & INTERFACES

Research Article

www.acsami.org

Role of Polyaniline on the Photocatalytic Degradation and Stability Performance of the Polyaniline/Silver/Silver Phosphate Composite under Visible Light

Yuyu Bu and Zhuoyuan Chen*

Key Laboratory of Marine Environmental Corrosion and Bio-fouling, Institute of Oceanology, Chinese Academy of Sciences, 7 Nanhai Road, Qingdao 266071, China

Supporting Information

ABSTRACT: Polyaniline/silver/silver phosphate (PANI/Ag/Ag_3PO_4) composite was prepared by in situ depositing silver phosphate (Ag_3PO_4) nanoparticles on the surface of polyaniline (PANI). The best photocatalytic Rhodamine B degradation performance is obtained by the 20 wt % PANI/Ag/Ag_3PO_4 composite, which is approximately 4 times higher than that of pure Ag_3PO_4. Meanwhile, the photocatalytic stability of Ag_3PO_4 is significantly improved by introducing PANI into the PANI/Ag/Ag_3PO_4 composite. The dramatic promotion of the photocatalytic degradation performance and the photocatalytic stability can be attributed to the formation of a heterojunction electric field between PANI and Ag_3PO_4, which is approximately 90 mV and points from Ag_3PO_4 to PANI. The existence of this electric field can dramatically enhance the separation efficiency of the photogenerated electron−hole pairs, accelerate the transfer of photogenerated holes from Ag_3PO_4 to PANI and therefore inhibit the self-oxidation of Ag_3PO_4.

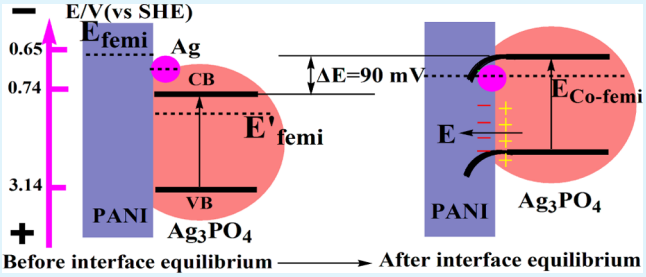

KEYWORDS: *silver phosphate, polyaniline, heterojunction, photocatalytic stability, visible light*

1. INTRODUCTION

Direct use of solar energy to address the issues of energy shortage and environmental pollution is one of the most promising technologies.[1,2] In the recent 40 years, the researchers have devoted themselves to this area and have greatly promoted the development of this field. However, the low quantum yield and the weak response of photocatalyst in visible light region are still hampering its wide application. Therefore, developing highly efficient visible light responsive photocatalysts with high quantum yields is the key to break the bottleneck of this technology.[3−6] Ag_3PO_4 has been reported possessing good visible-light photocatalytic property. Bi et al.[7] verified that Ag_3PO_4 with a rhombic dodecahedron structure showed a super high photocatalytic property. Subsequently, much work has systematically studied the photocatalytic property of Ag_3PO_4 and has confirmed that the photocatalytic property of Ag_3PO_4 is obviously better than that of other currently used visible-light responsive photocatalysts.[8−11] Recently, Ansari et al.[12] prepared Ag/TiO_2@Polyaniline nanocomposite film, and they found that this composite material possessed very strong visible light induced photocatalytic capability. Preparing graphene on the surface of Ag_3PO_4 can also efficiently enhance the photocatalytic performance of Ag_3PO_4 due to the super high electron migration rate of graphene and the heterojunction electric field formed on the interface of graphene and Ag_3PO_4.[13−15] Huang et al.[16] prepared series Ag@silver salt photocatalysts, and they found that the photocatalytic performance of these photocatalysts is related with the stability and the charge of the anion in the silver salts. Yu et al.[17] prepared Ag_3PO_4 nanoparticles on PAN fiber by ion exchange method and they found that the heterojunction system could significantly enhance the photocatalytic performance of the PAN/Ag_3PO_4 composite. However, Ag_3PO_4 itself has a relatively weak photocatalytic stability. The photogenerated holes by Ag_3PO_4 possess very high oxidation capability, which play a major role in the photocatalytic degration process of Ag_3PO_4. If the photoinduced holes generated by Ag_3PO_4 cannot swiftly consume away by reacting with the surrounding electrolyte or transferring to other materials, they will quickly oxidize Ag_3PO_4, leading to a rapid photoinduced corrosion of Ag_3PO_4 and a fast decay of the photocatalytic property of Ag_3PO_4. Therefore, the photocatalytic stability of Ag_3PO_4 need to be further improved.[18−23]

As a most intensively studied conductive polymer material, PANI has many applications in the catalytic and photocatalytic area.[24−28] PANI is a kind of π-conjugate long-chain polymer and the protonic acid doped PANI possesses very high conductivity. Meanwhile, PANI has three redox states: leucoemeraldine base, emeraldine base, and pernigraniline

Received: June 7, 2014
Accepted: September 22, 2014
Published: September 22, 2014

base, in which the leucoemeraldine base PANI possesses a weak reduction capability because of the existence of −NH− bonds for connecting the benzene rings.[29,30] A p−n heterojunction electric field will be built at the interface if PANI composites with an n-type semiconductor material. Under the influence of this electric field, the photogenerated holes will be swiftly transferred to PANI and oxidize the surrounding materials, while the photogenerated electrons will be rapidly transferred to the composited n-type semiconductor material and cause reduction reactions on the surface of this n-type semiconductor material. Zhang et al.[31] prepared a PANI@ZnO composite with quasi-shell−core structure by coating a PANI layer with the thickness of approximately 0.717 nm on the surface of ZnO. They reported that the PANI coating can significantly enhance the photocatalytic property of ZnO and inhibit the photocorrosion of ZnO. They attribute these benefits to the strong photogenerated hole trapping capability of PANI. The photogenerated holes can be rapidly transferred to π-conjugated PANI leading to the slowing down of the photocorrosion of ZnO. Therefore, the PANI/Ag/Ag_3PO_4 composite is expected to exhibit improved performance as a highly efficient visible light responsive photocatalyst.

In this work, PANI with branch-like structure was prepared, and subsequently Ag_3PO_4 nanoparticles were in situ grown on the surface of PANI. During the in situ growth of Ag_3PO_4 nanoparticles, some metallic Ag (Ag^0) was formed on the surface of PANI, resulting in the formation of PANI/Ag/Ag_3PO_4 composite. Subsequently, the photocatalytic degradation and stability performance of the prepared PANI/Ag/Ag_3PO_4 composites was studied in this paper.

2. EXPERIMENTAL SECTION

2.1. Preparation of PANI and the PANI/Ag/Ag_3PO_4 Composites. Aniline [0.046 g (5×10^{-4} mol)] and 0.036 g (1×10^{-4} mol) of cetyltrimethylammonium bromide (CTAB) were dissolved into 8.0 mL of deionized water, followed by dropwise adding 1.0 mL of 0.5 mol·L^{-1} HCl and 1.0 mL of 0.5 mol·L^{-1} ammonium peroxydisulfate. The mixture was kept at room temperature for 24 h. PANI precipitation was obtained by suction filtration. The precipitation was then rinsed with deionized water and acetone, and the PANI sample was obtained after 24 h of vacuum drying at 65 °C.

The PANI/Ag/Ag_3PO_4 composite was obtained by in situ depositing Ag_3PO_4 nanoparticles on the surface of the prepared PANI. First, 0.1 g of prepared PANI was dispersed into 25 mL of deionized water and the resulting mixture was ultrasonically vibrated for 5 min. A certain amount of $AgNO_3$, which was decided by the weight percentage of PANI in the PANI/Ag/Ag_3PO_4 composite, was added into this mixture and the liquid mixture was stirred for 1 h. A certain amount of Na_3PO_4, which is equal to 33.33% (in mole percentage) of the added $AgNO_3$ in the liquid mixture, was dissolved into 25 mL deionized water. The prepared Na_3PO_4 solution was then slowly added drop by drop into the liquid mixture of PANI and $AgNO_3$ under stirring. The solution was then stirred for 5 h. After that, the liquid mixture was centrifugalized and the centrifugate was repeatedly washed with anhydrous ethanol and deionized water. The PANI/Ag/Ag_3PO_4 composites with 16.67, 20, 25, 30, 40, and 50 wt % of PANI in them, which were expressed as 16.67 wt % PANI/Ag/Ag_3PO_4 composite, 20 wt % PANI/Ag/Ag_3PO_4 composite, 25 wt % PANI/Ag/Ag_3PO_4 composite, 30 wt % PANI/Ag/Ag_3PO_4 composite, 40 wt % PANI/Ag/Ag_3PO_4 composite, and 50 wt % PANI/Ag/Ag_3PO_4 composite, respectively, were obtained after drying at 55 °C for 24 h under vacuum conditions in this work. All reagents used in this study are analytical ones from Aladdin Reagent Corporation, China (Shanghai, China).

2.2. Characterizations of the Prepared PANI/Ag/Ag_3PO_4 Composites. The morphologies and the microstructure of the synthetic products were analyzed using a scanning electron microscopy (SEM) (SEM, JSM-6700F, JEOL, Japan) and a high-resolution transmission electron microscopy (HRTEM, Tecnai G2 F20, FEI Company, U.S.A.). The elemental compositions, elemental maps, the crystalline structures and bonding information on the synthetic products were analyzed using an energy dispersive spectrometry (EDS, INCA Energy, Oxford Instrument), HRTEM, X-ray diffraction (XRD, D/MAX-2500/PC, Rigaku Co., Tokyo, Japan), and X-ray photoelectron spectroscopy (XPS, Axis Ultra, Kratos Analytical Ltd., England). The optical absorption properties were investigated using a UV/vis diffuse reflectance spectrophotometer (U-41000; HITACHI, Tokyo, Japan). The photoluminescence intensity of the prepared samples was characterized using a fluorescence spectrometer (PL, Fluoro Max-4, HORIBA Jobin Yvon, France). The Brunauer−Emmett−Teller surface area was determined by a multipoint BET method (BET, 3Flex, Micromeritics, U.S.A.).

2.3. Photocatalytic Rhodamine B (RhB) Degradation. Prepared photocatalyst (0.1 g) was added to 100 mL RhB with a concentration of 10 mg·L^{-1} and stirred for 30 min in the dark. The light source was a 300 W xenon lamp (PLS-SXE300, Beijing Changtuo Co. Ltd., Beijing, China). A 420 nm cutoff filter was used to remove light with wavelengths less than 420 nm and ultimately generate visible light (power energy density is 150 mW/cm^2). All of the photocatalytic degradation measurements were performed under visible light. The distance between the light source and the dye liquid level is 10 cm. The temperature of the dye liquid was maintained at 25 °C using circulating water. The stability of the photocatalytic RhB degradation of the 20 wt % PANI/Ag/Ag_3PO_4 composite was studied in this work. The 20 wt % PANI/Ag/Ag_3PO_4 composite was recycled by the centrifugation of the solution after dye degradation at a centrifugal speed of 10000 r·min^{-1}, and the photocatalyst was used for the next cycle of the RhB degradation after sufficiently drying. The times of the photocatalyst recycling are 5.

2.4. Photoelectrode Preparation. The Ag_3PO_4 and the 20 wt % PANI/Ag/Ag_3PO_4 thin-film photoelectrodes were prepared in this work. An FTO glass (13 × 10 mm) was first ultrasonically cleaned with acetone of analytical grade for 5 min, rinsed with deionized water, and then dried with a clean, dry airflow. One longitudinal edge of the conductive side was then carefully covered with insulating tape, with the exposed effective area of the FTO glass measuring 1 cm^2. In total, 0.01 g of the prepared powder was mixed with 0.1 mL of deionized water in an agate mortar, and the mixture was carefully ground for 10 min to form a homogeneous suspension. Then, 0.025 mL of as-prepared suspension was evenly distributed onto the exposed area of the conductive side of the FTO glass. The insulating tape on the edge of the FTO glass was removed after the suspension dried in the air. Finally, the FTO glass deposited with the as-prepared suspension was heated to 120 °C for 2 h under vacuum condition. A copper wire was connected to the conductive side of the FTO glass using conductive silver tape. Uncoated parts of the conductive side of the FTO glass were isolated with parafilm after the conductive silver tape had dried.

2.5. Photoelectrochemical Measurements. Photoelectrochemical measurements were performed in a three-electrode experimental system using CHI660D Electrochemical Workstation (Shanghai Chenhua Instrument Co., Ltd., Shanghai, China). The prepared series photoelectrodes, saturated calomel electrode (SCE), and Pt electrode acted as the working, reference and counter electrodes, respectively. The potentials are reported on the SCE scale. The electrolyte was 0.1 mol·L^{-1} Na_2SO_4. Both the electrochemical impedance spectroscopy curves and the Mott−Schottky plots were measured in the dark. EIS tests were performed at open circuit potential over the frequency range between 10^4 and 10^{-1} Hz, with an AC voltage magnitude of 5 mV, using 12 points/decade. Mott−Schottky plots were measured at the potential range −1.0∼1.0 V, the frequency of 10 Hz with an AC voltage magnitude of 10 mV, and a scan rate of 5 mV·s^{-1}. The photogenerated current densities were measured at a bias potential of 0.5 V (vs SCE) in 0.1 mol·L^{-1} Na_2SO_4 under visible light on and off.

3. RESULTS AND DISCUSSION

Figure 1 shows the XRD patterns of the prepared Ag_3PO_4 particles and the PANI/Ag/Ag_3PO_4 composites with different

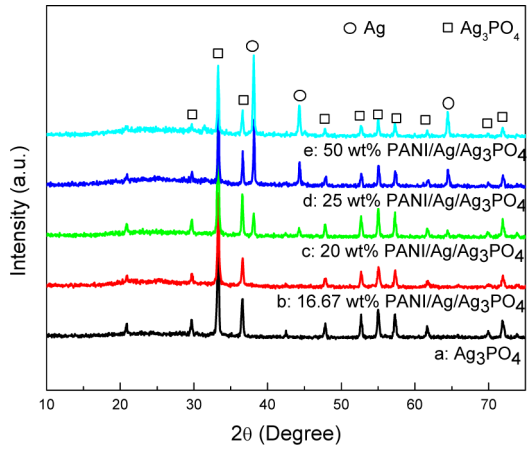

Figure 1. XRD patterns of Ag_3PO_4 (curve a), the 16.67 wt % PANI/Ag/Ag_3PO_4 composite (curve b), the 20 wt % PANI/Ag/Ag_3PO_4 composite (curve c), the 25 wt % PANI/Ag/Ag_3PO_4 composite (curve d), and the 50 wt % PANI/Ag/Ag_3PO_4 composite (curve e).

weight percent of PANI. Curve 1a is the XRD pattern of the prepared Ag_3PO_4, from which the crystal structure of the prepared Ag_3PO_4 is indexed as a cubic structure (JCPDS No. 06-0505). Curve 1b is the XRD pattern of the prepared 16.67 wt % PANI/Ag/Ag_3PO_4 composite. By comparing with curve 1a, there is no difference in the locations for the diffraction peaks of Ag_3PO_4 and the 16.67 wt % PANI/Ag/Ag_3PO_4 composite, demonstrating that the introduction of a small amount of PANI does not affect the crystal form and composition of Ag_3PO_4. Curve 1c is the XRD pattern of the prepared 20 wt % PANI/Ag/Ag_3PO_4 composite. In addition to the diffraction peaks from Ag_3PO_4, the diffraction peaks at 38.1°, 44.1°, and 64.4°, which are marked as "○" in curve 1c, can be readily indexed as the (111), (200), and (220) crystallographic planes of metallic Ag (JCPDS No. 04-0783), respectively. The intensities of the diffraction peaks from Ag^0 gradually increase with the further increase of the PANI weight percent, as shown in curves 1d and 1e, illustrating that PANI is helpful to the reduction of Ag^+ to Ag^0 to a certain extent. The prepared PANI in this work may exist as leucoemeraldine base and it possesses weak reducibility. When Ag^+ combines with —NH— groups in the PANI molecular chain, Ag^+ can oxidize the —NH— group to —N═ group and Ag^+ itself is reduced to Ag^0 on PANI surface, resulting in the formation of Ag^0.[32,33] The diffraction peaks of Ag_3PO_4 are observed in curves 1d and 1e, as those shown in curves 1a−1c. The above XRD results demonstrate that the composite is existed as PANI/Ag/Ag_3PO_4 when the amount of PANI in this composite is equal to or larger than 20 wt %. No characteristic diffraction peaks corresponding to those of PANI are observed in the curves 1b−1e, demonstrating that the PANI in the composites exists in amorphous form.

Figure 2 shows the UV/vis diffuse reflectance spectra of Ag_3PO_4 and the PANI/Ag/Ag_3PO_4 composite with different weight percentage of PANI. As the results shown in Figure 2, the light absorption intensity decreases with the increase of the weight percentage of the PANI in the composite, illustrating that Ag_3PO_4 possesses very strong light absorption capability

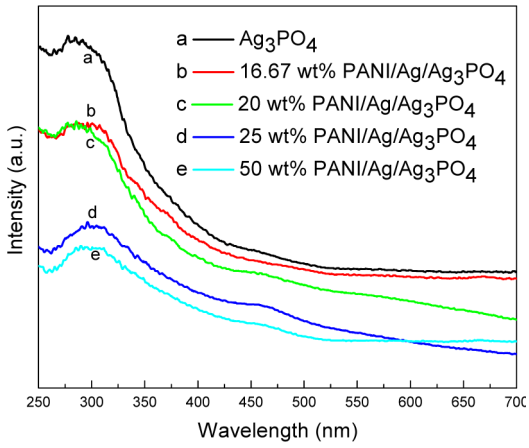

Figure 2. UV/vis diffuse reflectance spectra of Ag_3PO_4 (a), the 16.67 wt % PANI/Ag/Ag_3PO_4 composite (b), the 20 wt % PANI/Ag/Ag_3PO_4 composite (c), the 25 wt % PANI/Ag/Ag_3PO_4 composite (d), and the 50 wt % PANI/Ag/Ag_3PO_4 composite (e).

and PANI has very weak light absorption capability. The more the weight percentage of PANI in the composite is, the weaker the light absorption capacity of the PANI/Ag/Ag_3PO_4 composite is. When overmuch PANI is in the composite, competitive light absorption will be formed between PANI and Ag_3PO_4, leading to the decrease of the light absorption capability of this composite.

Figure 3 shows the SEM images of Ag_3PO_4 and the PANI/Ag/Ag_3PO_4 composites with different PANI weight percent (16.67%, 20%, and 50%) and the EDS results of the 20 wt % PANI/Ag/Ag_3PO_4 composite. The SEM image of the prepared Ag_3PO_4 nanoparticles in Figure 3a shows that the Ag_3PO_4 particles mainly exist in the form of agglomeration, which will decrease the number of the active photocatalytic reaction sites and cause a negative influence on the processes of the dye adsorption and the photocatalytic degradation. Figure 3b shows the SEM image of the 16.67 wt % PANI/Ag/Ag_3PO_4 composite. The agglomeration of Ag_3PO_4 particles is suppressed to a certain extent after introducing PANI into this composite. Because the amount of PANI in this composite is not high enough, PANI is not directly observed in Figure 3b, demonstrating that a thick coating layer of Ag_3PO_4 covers on the surface of PANI. Figure 3c shows the SEM image of the 20 wt % PANI/Ag/Ag_3PO_4 composite. Ag_3PO_4 particles are more uniformly distributed on the surface of PANI and PANI can be clearly observed. By increasing the PANI content to 50 wt %, the coverage of Ag_3PO_4 particles on PANI is further decreased and a lot of PANI is not covered by Ag_3PO_4 particles, as shown in Figure 3d. SEM images with high magnification (50000×) are inserted into each SEM picture listed in Figure 3a−d. By comparing these morphologies, it can be found that the dispersing capacity of Ag_3PO_4 particles on PANI surface tends to increase with the increase of PANI amount. This may be due to the increase of the adsorption site of Ag^+ with the increase of PANI amount in this composite, resulting in the increase of the particle dispersion of Ag_3PO_4 on PANI surface. Figure 3e shows the EDS results of the 20 wt % PANI/Ag/Ag_3PO_4 composite. The elements of C, N, O, P, and Ag are observed in the EDS results, which meet the element compositions of the PANI/Ag/Ag_3PO_4 composite.

In order to further study the loading information on Ag_3PO_4 particles on the PANI surface, the 20 wt % PANI/Ag/Ag_3PO_4

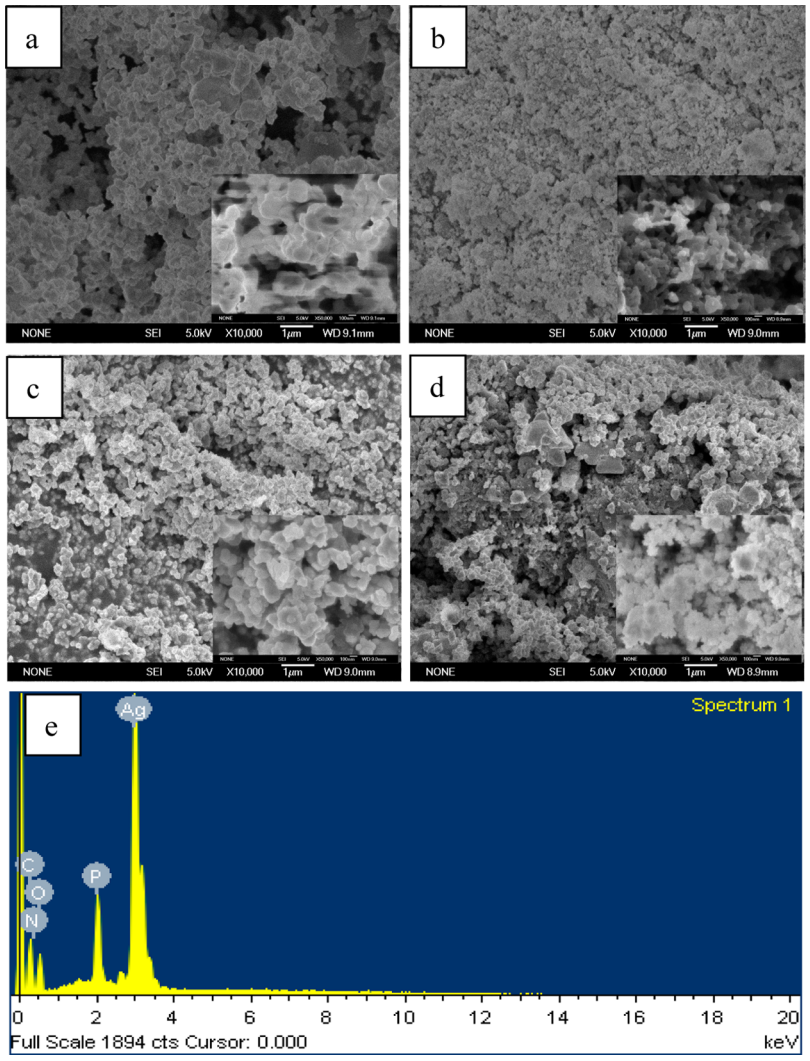

Figure 3. SEM images of (a) Ag_3PO_4, (b) the 16.67 wt % PANI/Ag/Ag_3PO_4 composite, (c) the 20 wt % PANI/Ag/Ag_3PO_4 composite, (d) the 50 wt % PANI/Ag/Ag_3PO_4 composite, and (e) the EDS results of the 20 wt % PANI/Ag/Ag_3PO_4 composite.

composite was selected for HRTEM investigations, and the relevant results are shown in Figure 4. Figure 4a shows the microscopic morphology under low magnification, from which PANI is observed existing as an irregular branch-like structure and a large number of Ag_3PO_4 particles with diameter of less than 50 nm are uniformly distributed on the surface of PANI. With the further increase of the magnification, the Ag_3PO_4 particles can be clearly observed distributing on the surface of PANI, as shown in Figure 4b. Figure 4c shows the HRTEM microscopic morphology of the distribution of Ag_3PO_4 particles on the surface of PANI under high magnification. The interplanar spacings of 0.299 and 0.268 nm are clearly observed, which correspond to (200) and (210) crystallographic planes of Ag_3PO_4, respectively. This is in good agreement with the JCPDS card No. 06-0505. The elemental maps of the 20 wt % PANI/Ag/Ag_3PO_4 composite were performed using TEM and the relevant results are shown in Figure 5. The results shown in Figure 5 can confirm that Ag_3PO_4 distributes on the surface of PANI.

XPS was further used to investigate the states of silver, phosphorus, and nitrogen in the prepared 20 wt % PANI/Ag/Ag_3PO_4 composite and Figure 6 shows the XPS spectra of the 20 wt % PANI/Ag/Ag_3PO_4 composite. The total survey spectrum in Figure 6a shows that P, C, N, O, and Ag are existed. Figure 6b shows the Ag 3d XPS core level spectrum. The binding energy peaks at 373.5 and 367.5 eV are assigned to the electron orbits of Ag $3d_{3/2}$ and Ag $3d_{5/2}$. After decomposing these two binding energy peaks at 373.5 and 367.5 eV by curve fitting, it can be found that the strong binding energy peaks at 373.5 and 367.5 eV are attributed to Ag^+, while the other two weak binding energy peaks at 374.2 and 368.3 eV are assigned to Ag^0, as shown in Figure 6b.[34,35] Figure 6c shows the P 2p XPS core level spectrum. The binding energy peak at 133.1 eV is assigned to the electron orbit of P 2p. Figure 6d shows the N 1s core level spectrum. The binding energy peak at 399.6 eV is assigned to C═N group, illustrating that the C—NH groups is oxidized to C═N groups by Ag^+, and Ag^+ is reduced to Ag^0 during the synthesis of the 20 wt % PANI/Ag/Ag_3PO_4 composite. The XPS results show that the PANI/Ag/Ag_3PO_4 composite with a little amount of metallic Ag as the intermediate layer was successfully synthesized when the amount of PANI in this composite is 20 wt %.

The RhB photocatalytic degradation capability of Ag_3PO_4 and PANI/Ag/Ag_3PO_4 composites were measured, as shown in the degradation curves in Figure 7. Curve 7a is the RhB degradation curve of the prepared Ag_3PO_4. Ag_3PO_4 exhibits a

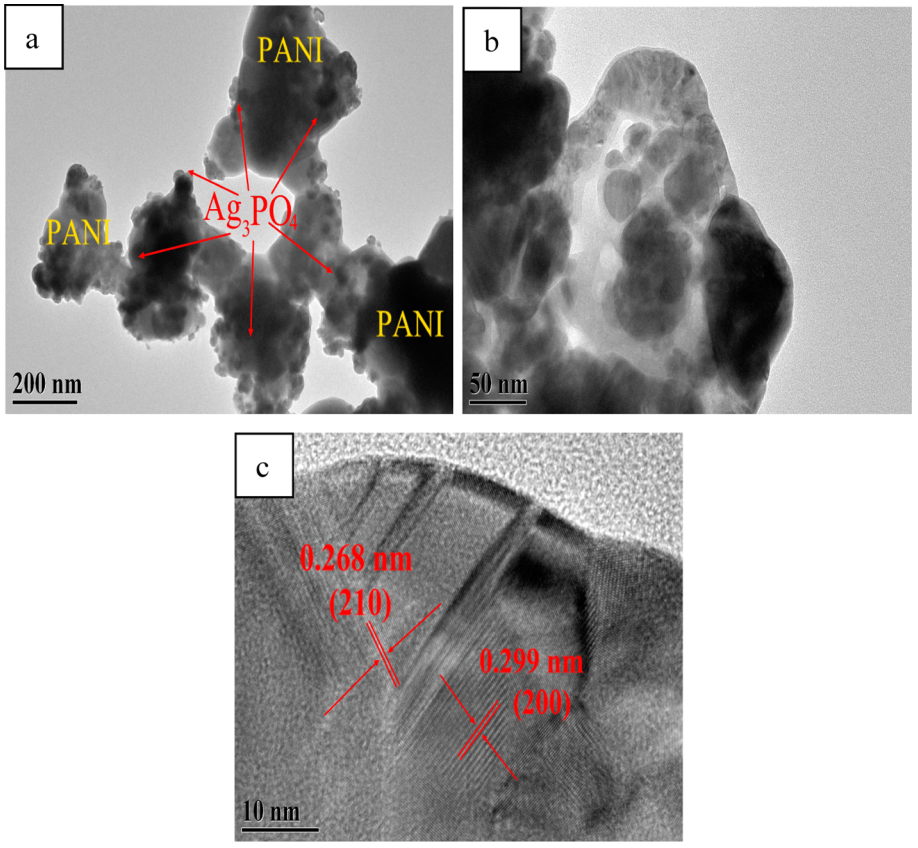

Figure 4. HRTEM images of the 20 wt % PANI/Ag/Ag_3PO_4 composite under (a) low, (b) medium, and (c) high magnifications.

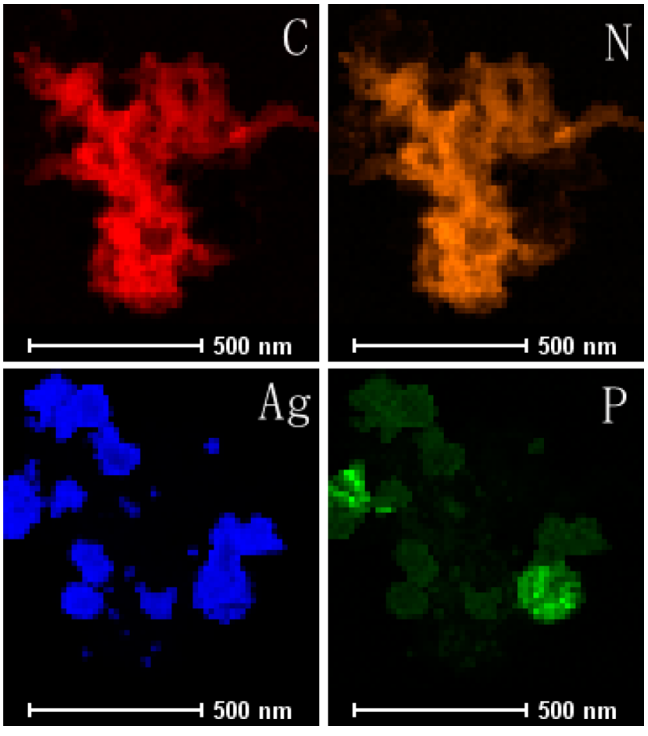

Figure 5. HRTEM elemental maps (C, N, Ag, P) of the 20 wt % PANI/Ag/Ag_3PO_4 composite.

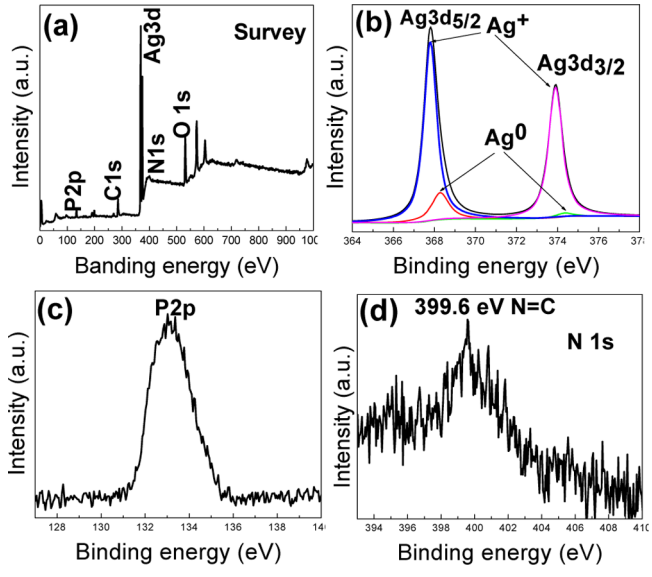

Figure 6. XPS spectra of the 20 wt % PANI/Ag/Ag_3PO_4 composite. (a) The total survey spectrum, (b) the Ag 3d XPS core level spectrum, (c) the P 2p XPS core level spectrum, and (d) the N 1s XPS core level spectrum.

very strong photocatalytic degradation capability under visible light illumination, and it takes only 20 min for the photocatalyst of Ag_3PO_4 to degrade all of the RhB dye. Curve 7b is the RhB degradation curve of the 50 wt % PANI/Ag/Ag_3PO_4 composite. As mentioned in the Experimental Section, the photocatalysts were mixed with the RhB solution in the dark and stirred for 30 min before the light was switched on. The introducing of PANI in the composite significantly improves the dye adsorption capacity of Ag_3PO_4. According to the data obtained from the 30 min adsorption in the dark, about 55%

dx.doi.org/10.1021/am503578s | ACS Appl. Mater. Interfaces 2014, 6, 17589−17598

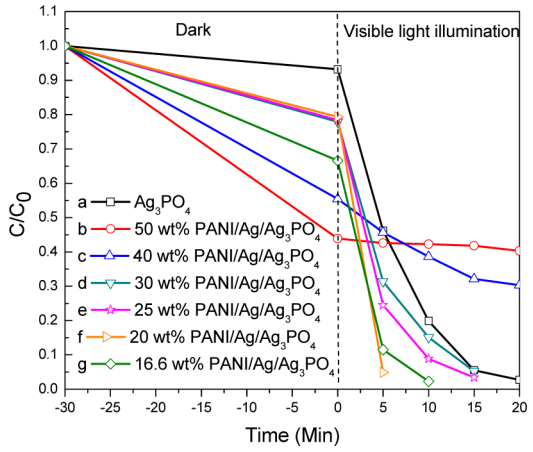

Figure 7. Photocatalytic RhB degradation efficiency of Ag_3PO_4 (a), the 50 wt % PANI/Ag/Ag_3PO_4 composite (b), the 40 wt % PANI/Ag/Ag_3PO_4 composite (c), the 30 wt % PANI/Ag/Ag_3PO_4 composite (d), the 25 wt % PANI/Ag/Ag_3PO_4 composite (e), the 20 wt % PANI/Ag/Ag_3PO_4 composite (f), and the 16.67 wt % PANI/Ag/Ag_3PO_4 composite (g) under visible light (λ > 420 nm) illumination.

RhB is adsorbed by the 50 wt % PANI/Ag/Ag_3PO_4 composite, as shown in curve 7b. However, the 50 wt % PANI/Ag/Ag_3PO_4 composite shows extremely poor photocatalytic RhB degradation performance under visible light illumination and no significant changes in the concentration of RhB can be found during the subsequent 20 min visible light illumination. The dye adsorption capacity of the PANI/Ag/Ag_3PO_4 composite decreases, while the photocatalytic RhB degradation performance of the PANI/Ag/Ag_3PO_4 composite increases with the decrease of the weight percent of PANI in this composite from 50% to 25%, as shown in the dye adsorption and photocatalytic degradation curves b, c, d, and e in Figure 7. This result demonstrates that PANI can enhance the adsorption ability of dyes and a large amount of RhB dye can be adsorbed on the surface of photocatalyst. Because of its strong light absorption ability, PANI and the adsorbed RhB will hinder the light absorption by Ag_3PO_4, resulting in the decrease of the photocatalytic RhB degradation performance of the PANI/Ag/Ag_3PO_4 composite with the increase of the PANI weight percent in this composite. For 25 wt % PANI/Ag/Ag_3PO_4 composite, it takes only 15 min to degrade all of the RhB dye, as shown in curve 7e. For 20 wt % PANI/Ag/Ag_3PO_4 composite, more than 95% RhB dye is degraded in 5 min, as shown in curve 7f. By comparing with curve 7a, the photocatalytic RhB degradation performance of the 20 wt % PANI/Ag/Ag_3PO_4 composite is much higher than that of Ag_3PO_4. With the further decrease of the weight percentage of PANI in the composite, the photocatalytic RhB degradation performance decreases. As shown in curve 7g, it takes 10 min to degrade all of the RhB dye for the 16.67 wt % PANI/Ag/Ag_3PO_4 composite. The results mentioned above indicate that the photocatalytic RhB degradation performance of the PANI/Ag/Ag_3PO_4 composite is closely related to the weight percentage of PANI in the composite. Overmuch PANI will decrease the light absorption intensity of Ag_3PO_4. While, too little PANI is not conducive to the promotion of the photocatalytic degradation performance of Ag_3PO_4. Based on the photocatalytic RhB degradation data shown in Figure 7, the 20 wt % PANI/Ag/Ag_3PO_4 composite possesses the optimal photocatalytic degradation efficiency.

As the results shown in Figure 7, the 50 wt % PANI/Ag/Ag_3PO_4 composite possesses the strongest RhB adsorption capability in the PANI/Ag/Ag_3PO_4 composites. Does it imply that 50 wt % PANI/Ag/Ag_3PO_4 composite has the highest specific surface area? To clarify this question, the specific surface areas and nitrogen adsorption−desorption curves of Ag_3PO_4, 50 wt % PANI/Ag/Ag_3PO_4 composite and 20 wt % PANI/Ag/Ag_3PO_4 composite were measured, and the relevant results are shown in Supporting Information (SI) Figure S1. Based on the shapes of the nitrogen adsorption−desorption curves shown in SI Figure S1, all of these three materials can be classified as IV-type adsorption−desorption characteristic, demonstrating that these materials have the mesoporous structures, which are formed mainly by the stacking of these materials. Based on SI Figure S1, the specific surface areas can be calculated, and those of Ag_3PO_4, 50 wt % PANI/Ag/Ag_3PO_4 composite, and 20 wt % PANI/Ag/Ag_3PO_4 composite are 1.1, 0.6, and 2.7 $m^2 \cdot g^{-1}$, respectively. The specific surface area results demonstrate that the strongest adsorption capacity of 50 wt % PANI/Ag/Ag_3PO_4 composite does not come from the contribution of its specific surface area but come from the strong selective adsorption capacity of metallic Ag on the surface of PANI for the azo RhB dye, resulting in a significant increase of the RhB adsorption capacity of 50 wt % PANI/Ag/Ag_3PO_4 composite.

As we know, the stability of a photocatalyst determines its service lifetime and practical application value. Although Ag_3PO_4 possesses very good photocatalytic performance, its light stability is poor and it is prone to photoinduced corrosion during the photocatalytic degradation process, resulting in a quick drop of the photocatalytic performance and thus a negative impact on its photocatalytic performance. Figure 8

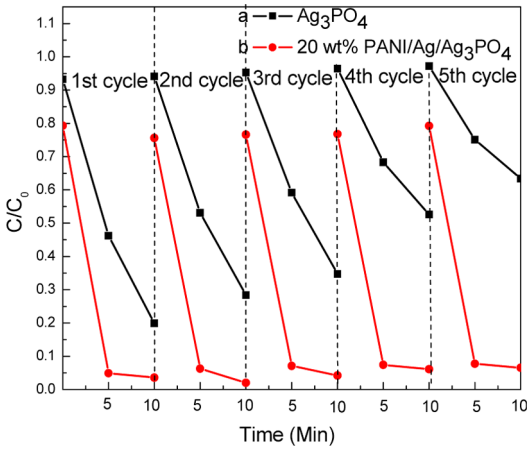

Figure 8. Stability study for the photocatalytic RhB degradation by Ag_3PO_4 (a) and the 20 wt % PANI/Ag/Ag_3PO_4 composite (b) under visible light (λ > 420 nm) illumination.

shows the photocatalytic RhB degradation stability of Ag_3PO_4 and the 20 wt % PANI/Ag/Ag_3PO_4 composite under visible light. Curve 8a shows the photocatalytic RhB degradation stability of Ag_3PO_4. In the first 10 min cycle, Ag_3PO_4 can degrade 80% RhB. With the increase of the cycles, its photocatalytic degradation performance continues to decrease, and only 40% RhB can be degraded at the fifth cycle. For the 20 wt % PANI/Ag/Ag_3PO_4 composite (curve 8b), in the first 10 min cycle, the 20 wt % PANI/Ag/Ag_3PO_4 composite can degrade 95% RhB in 5 min. Its photocatalytic degradation

performance does not exhibit any significant changes with the increase of the cycles. At the fifth cycle, the 20 wt % PANI/Ag/Ag_3PO_4 composite can still degrade 95% RhB in 5 min. Results shown in Figure 8 demonstrate that the introducing of PANI can significantly increase both the photocatalytic degradation performance and the photocatalytic degradation stability of Ag_3PO_4.

The scavengers of the photogenerated holes and electrons were added into the RhB dye solution to study the promotion mechanism of the photocatalytic degradation performance of the 20 wt % PANI/Ag/Ag_3PO_4 composite. Figure 9 shows the

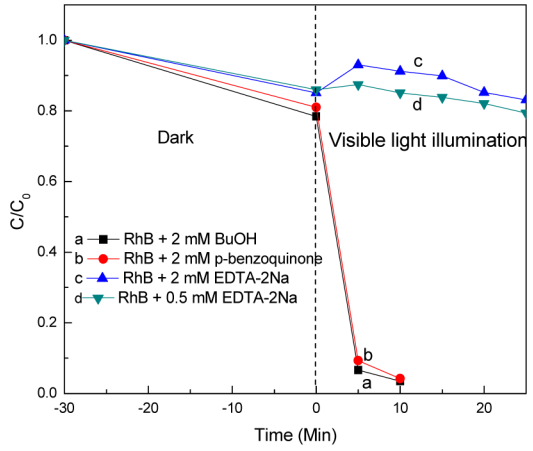

Figure 9. Photocatalytic RhB degradation efficiency of the 20 wt % PANI/Ag/Ag_3PO_4 composite in the RhB solution containing with 2 mM BuOH (a), 2 mM *p*-benzoquinone (b), 2 mM EDTA-2Na (c), or 0.5 mM EDTA-2Na (d), under visible light (λ > 420 nm) illumination.

photocatalytic RhB degradation curves of the 20 wt % PANI/Ag/Ag_3PO_4 composite in the RhB solution containing the scavenger of the photogenerated holes (EDTA-2Na), superoxide radicals (*p*-benzoquinone) or the photogenerated electrons (*tert*-butanol, BuOH).[36] Curve 9a is the RhB degradation curve of the 20 wt % PANI/Ag/Ag_3PO_4 composite in the RhB solution containing 2 mM BuOH. As we know, BuOH can capture the photogenerated electrons, leading to the swift consumption of the photogenerated electrons produced by the 20 wt % PANI/Ag/Ag_3PO_4 composite; therefore, the photogenerated electrons by the 20 wt % PANI/Ag/Ag_3PO_4 composite cannot contribute to the photocatalytic RhB degradation in the BuOH-containing RhB solution. As shown in curve 9a, the 20 wt % PANI/Ag/Ag_3PO_4 composite can degrade 95% RhB in 5 min and BuOH does not affect the photocatalytic RhB degradation performance of this composite, demonstrating that the photogenerated electrons does not play a role in the photocatalytic degradation process. Curve 9b is the RhB degradation curve of the 20 wt % PANI/Ag/Ag_3PO_4 composite in the RhB solution containing 2 mM *p*-benzoquinone, which is the capture agent for superoxide radicals. As shown in curve 9b, *p*-benzoquinone does not affect the photocatalytic RhB degradation performance of this composite, indicating that the photogenerated holes possess strong oxidation capability and they can directly participate into the RhB degradation processes. However, curve 9c indicates that the photocatalytic degradation performance of the 20 wt % PANI/Ag/Ag_3PO_4 significantly decreases by adding 2 mM EDTA-2Na composite in the RhB solution as compared with that in the RhB solution in the absence of EDTA-2Na (curve f in Figure 7) under visible light. Decreasing the EDTA-2Na to 0.5 mM (curve 9d), the photocatalytic degration performance of the 20 wt % PANI/Ag/Ag_3PO_4 composite in the RhB solution slightly recovers compared with that shown in curve 9c. The experimental results mentioned above reveal that the high photocatalytic degradation performance of the 20 wt % PANI/Ag/Ag_3PO_4 composite mainly comes from the strong oxidizing capability of the photogenerated holes.

The photoluminescence spectra can reflect, to some extent, the recombination efficiency of photogenerated electrons and holes by the fluorescence intensity. Secondary recombination of the photogenerated electrons and holes can occurred accompanied by the occurrence of the fluorescence. The strong intensity of the generated fluorescence means that the photogenerated electrons and holes are prone to recombination and the lifetime of the photogenerated electrons are short. However, the weak intensity of the generated fluorescence means that the separation efficiency of the photogenerated electrons and holes are high, resulting a longer lifetime of the photogenerated electrons and holes. Figure 10 shows the

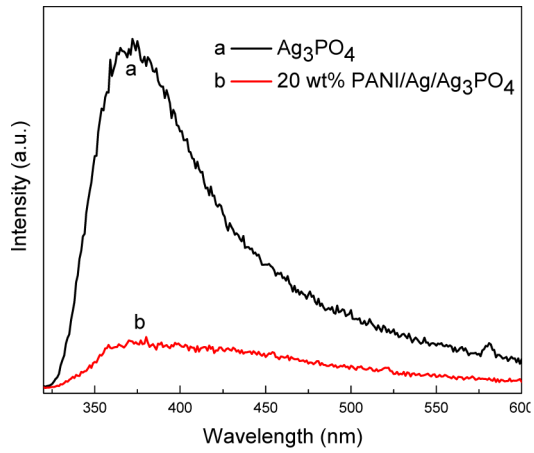

Figure 10. Photoluminescence spectra of Ag_3PO_4 (a) and the 20 wt % PANI/Ag/Ag_3PO_4 composite (b).

photoluminescence spectroscopy of Ag_3PO_4 and 20 wt % PANI/Ag/Ag_3PO_4. For Ag_3PO_4, a strong, luminous broad peak emerged at 300 to 500 nm. After compositing with 20 wt % PANI, the intensity of the luminous broad peak at 300 to 500 nm dramatically weakened, as shown in Figure 10, indicating that the presence of PANI can effectively inhibit the annihilation of the photogenerated electron−hole pairs and thus can effectively improve the separation efficiency and the lifetime of the photogenerated electrons and holes.

The separation efficiency of the photogenerated electrons and holes can also be supported from the photoinduced current densities data of the prepared photoelectrodes. SI Figure S2 shows the variations of the photogenerated current densities of the photoelectrodes prepared by Ag_3PO_4 and 20 wt % PANI/Ag/Ag_3PO_4 composite. As shown in SI Figure S2, the 20 wt % PANI/Ag/Ag_3PO_4 composite generates much larger photoinduced current density than Ag_3PO_4, demonstrating that the separation efficiency of the photogenerated electrons and holes and the migration ability of photogenerated electrons of Ag_3PO_4 are significantly increased due to the adding of PANI into this composite.

Figure 11 shows the EIS results and Mott−Schottky plots of Ag_3PO_4 and 20 wt % PANI/Ag/Ag_3PO_4 in 0.1 mol·L^{-1} Na_2SO_4

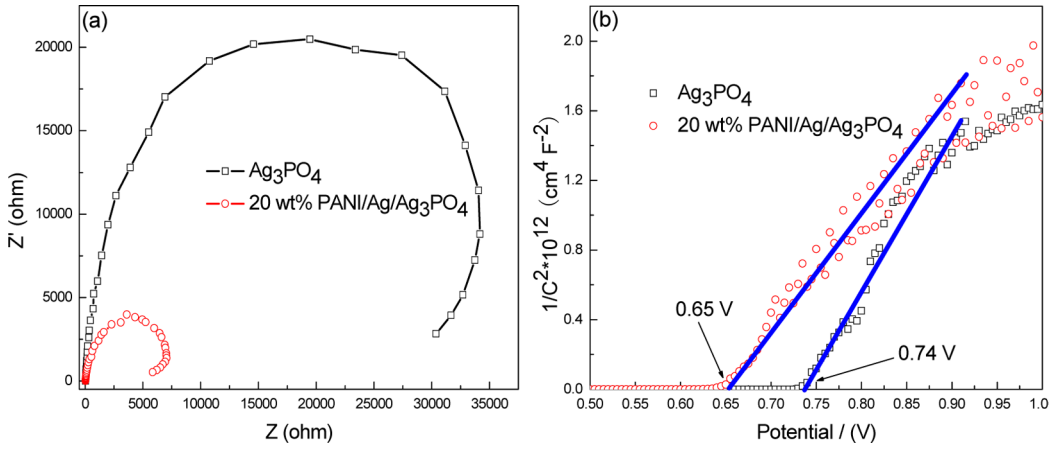

Figure 11. EIS spectra (a) and Mott−Schottky plots (b) of Ag_3PO_4 and the 20 wt % PANI/Ag/Ag_3PO_4 composite photoelectrodes in 0.1 mol·L^{-1} Na_2SO_4 solution in the dark.

solution in the dark. EIS can be used to study the migration ability and the interface reaction ability of the electrons in the photocatalytic materials, which are very closely related to the photocatalytic and photoelectrochemical properties of semiconductor materials. Figure 11a shows the EIS results, in which the vertical axis represents the imaginary part of the impedance, and the horizontal axis represents the real part of the impedance. The intercept of the semicircle arc of the EIS curve in the horizontal axis represents the actual value of the impedance, which is mainly decided by the exchange resistance of the photogenerated electrons on the interface between the electrolyte and the semiconductor material and the migration resistance of the photogenerated electrons and holes in the semiconductor material itself. As the results show in Figure 11a, the impedance value of Ag_3PO_4 is significantly larger than that of 20 wt % PANI/Ag/Ag_3PO_4 composite, illustrating that PANI can clearly promote the reaction ability of the photogenerated electrons and holes on the interface between the electrolyte and Ag_3PO_4 and increase the migration ability of the photogenerated electrons and holes in the composite.

Because the Fermi level of PANI is different from that of Ag_3PO_4, it is bound to cause movements of the Fermi levels of PANI and Ag_3PO_4 at the interface of these two materials, leading to the variations of the flat band potentials. In this paper, Mott−Schottky method was employed to study relation between the capacitance of the space charge region and the applied potential. The description of the specific formula is as follows:

$$1/C^2 = 2(e\varepsilon\varepsilon_0 N_D)^{-1}\,(E - E_{fb} - \kappa T/e) \quad (1)$$

where C is the capacitance of the space charge region in the semiconductor; N_D is the electron carrier density, e is the elemental charge, ε_0 is the permittivity of free space, ε is the relative permittivity of the semiconductor, E is the applied potential, E_{fb} is the flat band potential, T is the temperature, and κ is the Boltzmann constant.[37]

The flatband potential of a semiconductor material can be determined by extrapolating to $C^{2-} = 0$. Figure 11b shows the Mott−Schottky plots of Ag_3PO_4 and 20 wt % PANI/Ag/Ag_3PO_4. From the slopes of the tangent lines of the Mott−Schottky plots, both Ag_3PO_4 and 20 wt % PANI/Ag/Ag_3PO_4 show the characteristics of the n-type semiconductor. The flatband potentials of Ag_3PO_4 and 20 wt % PANI/Ag/Ag_3PO_4 were approximately 0.74 and 0.65 V, respectively (Figure 11b). Thus, the introducing of PANI onto the surface of Ag_3PO_4 negatively shifted the flatband potential, demonstrating that an interfacial electric field is built at the interface of PANI and Ag_3PO_4.

Figure 12 schematically shows the shift of the electron energy level due to the introducing of PANI into Ag_3PO_4. It is

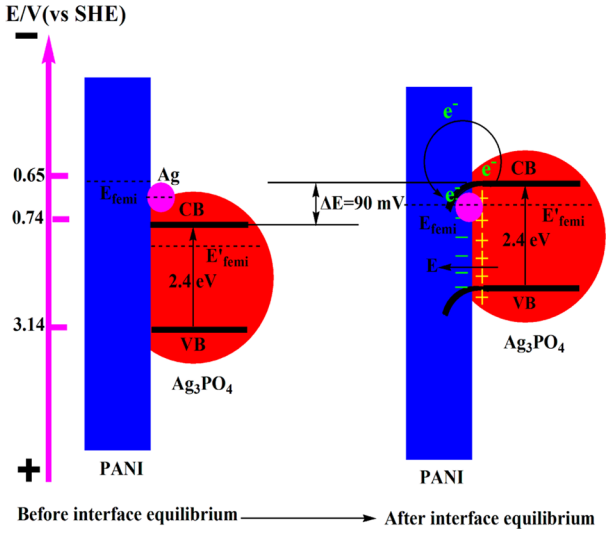

Figure 12. Schematic illustrations of the shift of the electron energy levels due to the introducing of PANI into Ag_3PO_4.

reported that the bandgap of Ag_3PO_4 is 2.4 eV and the valence band potential is approximately 3.14 V (vs SHE). Results shown in Figure 11b indicate that Ag_3PO_4 is an n-type semiconductor with the flatband potential of 0.74 V. The Fermi level of Ag_3PO_4 is just located below the conduction band; therefore, the Fermi level of Ag_3PO_4 is more positive than 0.74 V. While, the Fermi levels of PANI and Ag are much more negative than 0.74 V. By adding PANI and Ag to Ag_3PO_4, the Fermi levels of these three materials will move to each other and eventually reach to the same potential value with the Fermi level moving to negative direction for Ag_3PO_4 and to positive direction for PANI. The negative movement of the Fermi level of Ag_3PO_4 will also promote the negative movement of its conduction band and valence band. Because of the exchange of electrons and holes, the energy band of the surface layer bended downward, as a result of that, the electrons on the

surface of Ag_3PO_4 will transfer to the surface of PANI to form an electron rich layer there, and a hole rich layer will form on the surface of Ag_3PO_4 at the same time. Therefore, an electric field forms at the interface of Ag_3PO_4 and PANI and the direction of the electric field is pointed from Ag_3PO_4 to PANI. The intensity of this electric field is approximately equal to the energy level bend amount, which is approximately 90 mV.

The interfacial electric field, formed at the interface of Ag_3PO_4 and PANI, can promote the separation efficiency of photogenerated electrons and holes of Ag_3PO_4. Meanwhile, the direction of the electric field may also have contributed to the improvement of the photocatalytic stability of the PANI/Ag_3PO_4 composite. The relevant mechanism is schematically shown in Figure 13. The long chain of leucoemeraldine base

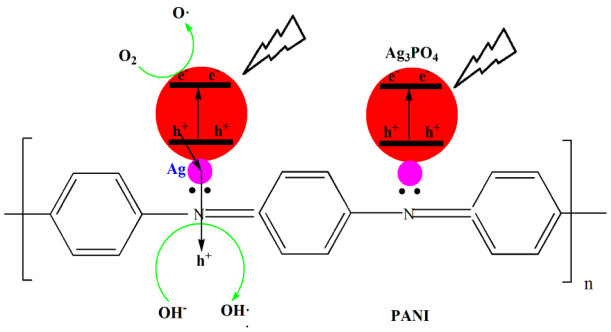

Figure 13. Proposed mechanism for the charge transfer of the photogenerated electrons and holes by Ag_3PO_4 in the PANI/Ag/Ag_3PO_4 composite under visible light illumination.

PANI is connected to each other by the —NH— bonds, and the N atoms in the outer layer are very easy to adsorb Ag^+ because of its strong negative lone-pair electrons. Then, the adsorbed Ag^+ oxidizes —C—NH— bond to —N=C— bond due to the weak reduction ability of leucoemeraldine base PANI, resulting in the formation of Ag^0. PO_4^{3+} will react with the adsorbed Ag^+ and Ag_3PO_4 particles is then in situ formed on the long chain of PANI. Under the excitation of incident light, Ag_3PO_4 generates photoinduced electrons and holes. As mentioned in Figure 12, an electric field is formed at the interface of PANI and Ag_3PO_4 and the direction of the electric field is pointed from Ag_3PO_4 to PANI. Therefore, the photogenerated holes by Ag_3PO_4 will swiftly transfer to PANI under this electric field and oxidize the surrounding electrolyte of PANI.[38,39] As we know, the valence band potential of Ag_3PO_4 is 3.14 V, indicating that the photogenerated holes by Ag_3PO_4 possess very strong oxidation capability. If these photogenerated holes cannot be quickly transferred from the bulk phase of Ag_3PO_4, they will definitely oxidize Ag_3PO_4 itself. Due to the existence of Ag^0 and PANI, the photogenerated holes can be quickly transferred to PANI bulk phase under the help of the heterojunction electric field at the interface of Ag_3PO_4 and PANI, thus avoiding the photocorrosion of Ag_3PO_4 itself. Meanwhile, the amount of the formed Ag^0 directly affects the separation efficiency of the photogenerated electrons and holes. A certain amount of Ag^0 is favorable for the separation of the photogenerated electrons and holes; however, overmuch Ag^0 will darken the color of this composite and compete with Ag_3PO_4 for the light absorption. Meanwhile, overmuch Ag^0 will turn into the recombination center of the photogenerated electrons and holes, resulting in the decrease of the photocatalytic performance of this composite.[40,41]

4. CONCLUSIONS

PANI/Ag/Ag_3PO_4 composites with very strong photocatalytic capability were successfully prepared by in situ formation of Ag_3PO_4 particles on PANI. The introducing of PANI in the PANI/Ag/Ag_3PO_4 composite can significantly increase both the photocatalytic degradation performance and the photocatalytic degradation stability of Ag_3PO_4. The photocatalytic degradation performance of the PANI/Ag/Ag_3PO_4 composite is closely related to the weight percent of PANI in the composite. The 20 wt % PANI/Ag/Ag_3PO_4 composite possesses the optimal photocatalytic degradation efficiency and only 5 min is needed to degrade more than 95% RhB dye. However, overmuch PANI will decrease the light absorption intensity of Ag_3PO_4, thus decreasing its photocatalytic degradation ability. The promotion of both the photocatalytic degradation performance and the photocatalytic stability of Ag_3PO_4 after introducing PANI into the PANI/Ag/Ag_3PO_4 composite are mainly due to the formation of the heterojunction electric field at the interface of Ag_3PO_4 and PANI. On one hand, the separation efficiency of the photogenerated electron−hole pairs and the lifetime of the photogenerated electrons are dramatically increased due to the formation of the heterojunction electric field at the interface of Ag_3PO_4 and PANI. On the other hand, the photogenerated holes produced by Ag_3PO_4 are swiftly transferred to PANI under the formed electric field at the interface of Ag_3PO_4 and PANI and therefore effectively slowing down the photocorrosion of Ag_3PO_4.

■ ASSOCIATED CONTENT

Ⓢ Supporting Information

BET and photogenerated current densities results. This material is available free of charge via the Internet at http://pubs.acs.org/.

■ AUTHOR INFORMATION

Corresponding Author

*Tel: +86 532 8289 8731. Fax: +86 532 8288 0498. Email: zychen@qdio.ac.cn.

Author Contributions

Both authors contributed equally.

Funding

National Natural Science Foundation of China (Grant No. 41376126) and the Hundreds-Talent Program of the Chinese Academy of Sciences (Y02616101L) were used to support the research of this paper.

Notes

The authors declare no competing financial interest.

■ ACKNOWLEDGMENTS

This work was financially supported by the National Natural Science Foundation of China (Grant No. 41376126) and the Hundreds-Talent Program of the Chinese Academy of Sciences (Y02616101L).

■ REFERENCES

(1) Abe, R. Recent Progress on Photocatalytic and Photoelectrochemical Water Splitting Under Visible Light Irradiation. *J. Photochem. Photobiol., C* **2010**, *11*, 179−209.

(2) Maeda, K.; Domen, K. Download Citations Photocatalytic Water Splitting: Recent Progress and Future Challenges. *J. Phys. Chem. Lett.* **2010**, *1*, 2655−2661.

(3) Fujishima, A.; Honda, K. Electrochemical Photolysis of Water at a Semiconductor Electrode. *Nature* **1972**, *238*, 37−38.
(4) Walter, M. G.; Warren, E. L.; McKone, J. R.; Boettcher, S. W.; Mi, Q.; Santori, E. A.; Lewis, N. S. Solar Water Splitting Cells. *Chem. Rev.* **2010**, *110*, 6446−6473.
(5) Kudo, A.; Miseki, Y. Heterogeneous Photocatalyst Materials for Water Splitting. *Chem. Soc. Rev.* **2009**, *38*, 253−278.
(6) Zhang, Z.; Yates, J. T., Jr Band Bending in Semiconductors: Chemical and Physical Consequences at Surfaces and Interfaces. *Chem. Rev.* **2012**, *112*, 5520−5551.
(7) Bi, Y.; Ouyang, S.; Umezawa, N.; Cao, J.; Ye, J. Facet Effect of Single-Crystalline Ag_3PO_4 Sub-Microcrystals on Photocatalytic Properties. *J. Am. Chem. Soc.* **2011**, *133*, 6490−6492.
(8) Lin, Y.; Hsu, Y.; Chen, Y.; Wang, S.; Miller, J. T.; Chen, L.; Chen, K. Plasmonic $Ag@Ag_3(PO_4)_{1-x}$ Nanoparticle Photosensitized ZnO Nanorod-Array Photoanodes for Water Oxidation. *Energy Environ. Sci.* **2012**, *5*, 8917−8922.
(9) Martin, D. J.; Umezawa, N.; Chen, X.; Ye, J.; Tang, J. Facet Engineered Ag_3PO_4 for Efficient Water Photooxidation. *Energy Environ. Sci.* **2013**, *6*, 3380−3386.
(10) Bi, Y.; Hu, H.; Ouyang, S.; Lu, G.; Cao, J.; Ye, J. Photocatalytic and Photoelectric Properties of Cubic Ag_3PO_4 Sub-Microcrystals with Sharp Corners and Edges. *Chem. Commun.* **2012**, *48*, 3748−3750.
(11) Zhang, H.; Huang, H.; Ming, H.; Li, H.; Zhang, L.; Liu, Y.; Kang, Z. Carbon Quantum Dots/Ag_3PO_4 Complex Photocatalysts with Enhanced Photocatalytic Activity and Stability under Visible Light. *J. Mater. Chem.* **2012**, *22*, 10501−10506.
(12) Ansari, M. O.; Khan, M. M.; Ansari, S. A.; Raju, K.; Lee, J.; Cho, M. H. Enhanced Thermal Stability under DC Electrical Conductivity Retention and Visible Light Activity of Ag/TiO_2@Polyaniline Nanocomposite Film. *ACS Appl. Mater. Interfaces* **2014**, *6*, 8124−8133.
(13) Peng, W.; Wang, X.; Li, X. Synergetic Effect of MoS_2 and Graphene on Ag_3PO_4 for its Ultra-Enhanced Photocatalytic Activity in Phenols Degradation under Visible Light. *Nanoscale* **2014**, *6*, 8311−8317.
(14) Cui, H.; Yang, X.; Gao, Q.; Liu, H.; Li, Y.; Tang, H.; Zhang, R.; Qin, J.; Yan, X. Facile Synthesis of Graphene Oxide-Enwrapped Ag_3PO_4 Composites with Highly Efficient Visible Light Photocatalytic Performance. *Mater. Lett.* **2013**, *93*, 28−31.
(15) Yang, X.; Qin, J.; Jiang, Y.; Li, Y.; Tang, H. Bifunctional TiO_2/Ag_3PO_4/Graphene Composites with Superior Visible Light Photocatalytic Performance and Synergistic Inactivation of Bacteria. *RSC Adv.* **2014**, *4*, 18627−18636.
(16) Huang, H.; Li, X.; Kang, Z.; Liu, Y.; Li, H.; He, X.; Lian, S.; Liu, J.; Lee, S. Tuning Metal@Metal Salt Photocatalytic Abilities by Different Charged Anions. *Dalton Trans.* **2010**, *39*, 10593−10597.
(17) Yu, H.; Dong, Q.; Jiao, Z.; Wang, T.; Ma, J.; Lu, G.; Bi, Y. Ion Exchange Synthesis of PAN/Ag_3PO_4 Core−Shell Nanofibers with Enhanced Photocatalytic Properties. *J. Mater. Chem. A* **2014**, *2*, 1668−1671.
(18) Xu, Y. S.; Zhang, W. D. Monodispersed Ag_3PO_4 Nanocrystals Loaded on the Surface of Spherical Bi_2MoO_6 with Enhanced Photocatalytic Performance. *Dalton Trans.* **2013**, *42*, 1094−1101.
(19) Yang, X.; Cui, H.; Li, Y.; Qin, J.; Zhang, R.; Tang, H. Fabrication of Ag_3PO_4-Graphene Composites with Highly Efficient and Stable Visible Light Photocatalytic Performance. *ACS Catal.* **2013**, *3*, 363−369.
(20) Liang, Q.; Shi, Y.; Ma, W.; Li, Z.; Yang, X. Enhanced Photocatalytic Activity and Structural Stability by Hybridizing Ag_3PO_4 Nanospheres with Graphene Oxide Sheets. *Phys. Chem. Chem. Phys.* **2012**, *14*, 15657−15665.
(21) Kumar, S.; Surendar, T.; Baruah, A.; Shanker, V. Synthesis of a Novel and Stable g-C_3N_4-Ag_3PO_4 Hybrid Nanocomposite Photocatalyst and Study of the Photocatalytic Activity under Visible Light Irradiation. *J. Mater. Chem. A* **2013**, *1*, 5333−5340.
(22) Yao, W.; Zhang, B.; Huang, C.; Ma, C.; Song, X.; Xu, Q. Photocorrosion Inhibition and Photoactivity Enhancement for Zinc Oxide via Hybridization with Monolayer Polyaniline. *J. Mater. Chem.* **2012**, *22*, 4050−4055.
(23) Zhang, L.; Zhang, H.; Huang, H.; Liu, Y.; Kang, Z. Ag_3PO_4/SnO_2 Semiconductor Nanocomposites with Enhanced Photocatalytic Activity and Stability. *New J. Chem.* **2012**, *36*, 1541−1544.
(24) Kang, E. T.; Neoh, K. G.; Tan, K. L. Polyaniline: A Polymer with Many Interesting Intrinsic Redox States. *Prog. Polym. Sci.* **1998**, *23*, 277−324.
(25) Shirota, Y.; Kageyama, H. Charge Carrier Transporting Molecular Materials and Their Applications in Devices. *Chem. Rev.* **2007**, *107*, 953−1010.
(26) Shang, M.; Wang, W.; Sun, S.; Ren, J.; Zhou, L.; Zhang, L. Download Citations Efficient Visible Light-Induced Photocatalytic Degradation of Contaminant by Spindle-like PANI/$BiVO_4$. *J. Phys. Chem. C* **2009**, *113*, 20228−20233.
(27) Zhang, H.; Zong, R.; Zhao, J.; Zhu, Y. Dramatic Visible Photocatalytic Degradation Performances due to Synergetic Effect of TiO_2 with PANI. *Environ. Sci. Technol.* **2008**, *42*, 3803−3807.
(28) Huang, H.; Liu, Y.; Lee, S.; Kang, Z. Polymer (Polyanilines) Nanoparticles: A Superior Catalyst for Hydrocarbon Selective Oxidation. *J. Mater. Chem.* **2012**, *22*, 337−340.
(29) Stejskal, J.; Sapurina, I.; Trchova, M. Polyaniline Nanostructures and the Role of Aniline Oligomers in their Formation. *Prog. Polym. Sci.* **2010**, *35*, 1420−1481.
(30) Dhand, C.; Das, M.; Datta, M.; Malhotra, B. D. Recent Advances in Polyaniline Based Biosensors. *Biosens. Bioelectron.* **2011**, *26*, 2811−2821.
(31) Zhang, H.; Zong, R.; Zhu, Y. Photocorrosion Inhibition and Photoactivity Enhancement for Zinc Oxide via Hybridization with Monolayer Polyaniline. *J. Phys. Chem. C* **2009**, *113*, 4605−4611.
(32) Bedre, M. D.; Basavaraja, S.; Salwe, B. D.; Shivakumar, V.; Arunkumar, L.; Venkataraman, A. Preparation and Characterization of Pani and Pani-Ag Nanocomposites via Interfacial Polymerization. *Polym. Compos.* **2009**, *30*, 1668−1677.
(33) Heeger, A. J. Semiconducting and Metallic Polymers: The Fourth Generation of Polymeric Materials. *J. Phys. Chem. B* **2001**, *105*, 8475−8491.
(34) Zhu, M.; Chen, P.; Liu, M. Visible-Light-Driven Ag/Ag_3PO_4-based Plasmonic Photocatalysts: Enhanced Photocatalytic Performance by Hybridization with Graphene Oxide. *Chin. Sci. Bull.* **2013**, *58*, 84−91.
(35) Chen, Z.; Wang, W.; Zhang, Z.; Fang, X. High-Efficiency Visible-Light-Driven Ag_3PO_4/AgI Photocatalysts: Z-Scheme Photocatalytic Mechanism for Their Enhanced Photocatalytic Activity. *J. Phys. Chem. C* **2013**, *207*, 19346−19352.
(36) Xu, T.; Zhang, L.; Cheng, H.; Zhu, Y. Significantly Enhanced Photocatalytic Performance of ZnO via Graphene Hybridization and the Mechanism Study. *Appl. Catal., B* **2011**, *101*, 382−387.
(37) Bu, Y.; Chen, Z.; Li, W. Using Electrochemical Methods to Study the Promotion Mechanism of the Photoelectric Conversion Performance of Ag-Modified Mesoporous g-C_3N_4 Heterojunction Material. *Appl. Catal., B* **2014**, *144*, 622−630.
(38) Wang, X.; Li, S.; Yu, H.; Yu, J.; Liu, S. Ag_2O as a New Visible-Light Photocatalyst: Self-Stability and High Photocatalytic Activity. *Chem.—Eur. J.* **2011**, *17*, 7777−7780.
(39) Liu, W.; Liu, X.; Fu, Y.; You, Q.; Huang, R.; Liu, P.; Li, Z. Nanocrystalline Pyrochlore $AgSbO_3$: Hydrothermal Synthesis, Photocatalytic Activity, and Self-Stable Mechanism Study. *Appl. Catal., B* **2012**, *123−124*, 78−83.
(40) Zheng, Y.; Zheng, L.; Zhan, Y.; Lin, X.; Zheng, Q.; Wei, K. Ag/ZnO Heterostructure Nanocrystals: Synthesis, Characterization, and Photocatalysis. *Inorg. Chem.* **2007**, *46*, 6980−6986.
(41) Sheng, F.; Xu, C.; Jin, Z.; Guo, J.; Fang, S.; Shi, Z.; Wang, J. Simulation on Field Enhanced Electron Transfer between the Interface of ZnO−Ag Nanocomposite. *J. Phys. Chem. C* **2013**, *117*, 18627−18633.